https://doi.org/10.2352/ISSN.2470-1173.2021.16.COLOR-339

Design and Fabrication of Microfluidics Paper-Based Devices for Contaminant Detection Using a Wax Printer

Qiyue Liang [1]***, Min Zhao*** [1]***, George T. C. Chiu*** [1]***, and Jan P. Allebach*** [1]
[1] ***Purdue University, West Lafayette, IN 47906, USA***

Abstract

In this paper, we introduce an eight-channel paper-based microfluidic device that aims to detect multiple chemicals at once. The microfluidic device we propose is fabricated by wax printing on filter paper, which is trouble-free to handle, low cost, and easy to fabricate. As a hydrophobic material, wax (solid ink) defines the hydrophilic channels for testing. By using image processing techniques, we analyze the width change caused by heating of wax strokes and wax channels, which is a necessary step in the wax printing fabrications. In the same way, we test the minimum width of a channel that allows solutions to cross through and the minimum width of a barrier that is hydrophobic and blocks liquid flow. We also compare two different heating methods, the heat gun and the hot plate, by checking the wax channel width before and after heating based on our image processing pipeline. We conclude that a heat gun will be better for heating channels with relatively large widths. Using high resolution wax printing, we integrate multiple devices on a single paper, which makes this method very cost-effective. Lamination of wax-printed paper based devices is also analyzed, as leakage on the back side of paper is sometimes worth attention.

Introduction

Food safety is a major concern for us, and we might want our food be tested with a portable and easy to use device to determine whether it contains harmful chemicals that can result in health risks. Paper based microfluidic devices have long been considered as suitable for doing quick tests and are capable of performing the required task under many different circumstances. This being said, our goal is to fabricate paper based microfluidic devices that can assess food safety for us. These devices will likely be used very frequently, so they must be affordable. In addition, we want our device to be able to detect multiple chemicals at the same time, because there might be multiple harmful chemicals in our foods. Therefore, for parallel tasking, we design and fabricate 8-channel paper-based devices. Fabrication is accomplished through wax printing because it is a low-cost, highly reproducible fabrication method with a relatively small batch-to-batch variation. Based on our image processing pipeline, we calibrate wax printing outputs in four steps. We also compare two generally used heating sources for the reflowing of wax printing outputs: heat gun and hot plate. We consider that daily users might not want leakage to be present on the backside of our devices. Therefore, we try to use both wax and lamination sheets to prevent leakage on the backside.

Related Works

Over the course of time, people have come up with a series of ways to fabricate paper based microfluidic devices. Some people used lithography to fabricate microfluidic devices [1], [2]. The most advantageous point of this type of fabrication method is probably the very high resolution, it often can go down to hundreds of nanometers or even below 100 nm. The materials used in lithography methods such as photoresists are generally inexpensive, but doing lithography may require some special types of equipment, and training people to do lithography will add to the total cost. People also proposed fabricating microfluidic devices with a desktop cutter [3], or by dropping hydrophilic droplets, most commonly Polydimethylsiloxane (PDMS), to the paper [4]. These types of methods are even cheaper and easier compared to lithography, but the process may not be that simple. For example, the usage of PDMS as a hydrophobic material requires a long curing time at a constant temperature. In addition, the resolution of devices fabricated by these types of fabrication methods may not be comparable to the devices fabricated with traditional lithography methods, and the batch-to-batch variance can be large. Another very popular way of fabricating microfluidic devices is screen printing. Our group have reported a four-channel paper based microfluidic device fabricated with screen printing method in 2020 [5]. For screen printing fabrication, UV-curable ink was used as the hydrophobic material to define the channels of the microfluidic device. Detection of heavy metal particles ($Hg2+$, $As3+$) from 0 to 100 ppm was successful with the low cost, screen-printed, four-channel microfluidic paper devices. This work takes our microfluidic devices one step further by fabricating devices with 8 channels using wax printing. Going from 4 channels to 8 channels, users are able to perform even more tests at once. Wax printing is chosen instead of screen printing when fabricating our 8-channel devices because wax printing has higher resolution than screen printing. Wax printing also makes prototyping new patterns easier because printing can be carried out in a shorter time. In addition, the printing process is performed automatically with a wax printer which is very handy. The idea of using a wax printer to fabricate paper based microfluidic devices was introduced in 2009 [6]. Since then, many researches have been conducted using this wax printing idea [7], [8], [9]. Reference [10] introduced the idea of using wax patterns for lamination and flow rate control. We are not particularly concerned with flow rate, but we are interested in lamination, so we try the idea of using wax for lamination.

Methods

The fabrication of a wax printing paper device involves two simple steps. The first step is to print wax on paper, in our case we

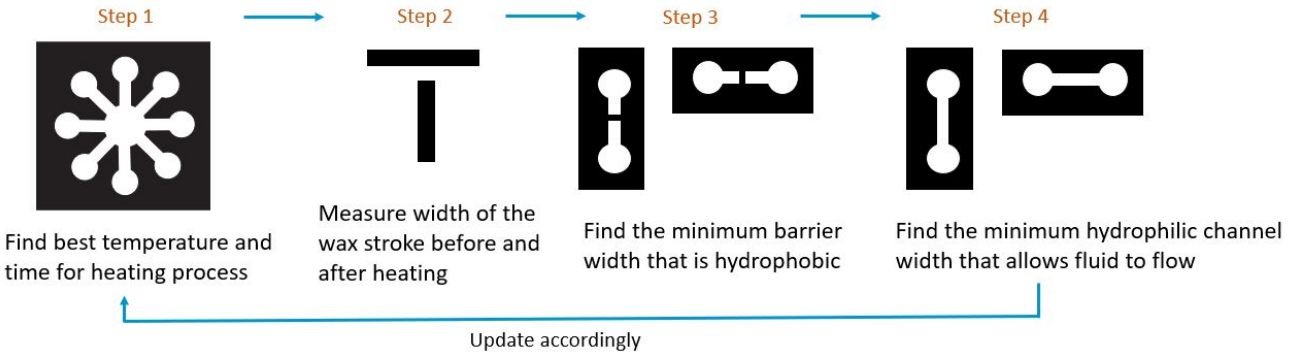

Figure 1: Experimental Flowchart for Printer Calibration. Step 1: Apply different temperatures (from 70 °C to 200 °C with 10 °C increment) to the draft 8-channel pattern and record the time (up to 5 mins) when the wax melts and forms a hydrophobic barrier. Step 2: From Step 1, select 3 best temperature and time combinations, measure the width of the hydrophobic barrier after heating. Use QEA Digital Microscope (Billerica, MA, USA) to take pictures and apply image analysis pipelines based on Ostu's threholding method [11]. Select the one best recipe (out of 3) from Step 2 based on standard deviation of width, use that best recipe for the following steps. Step 3: Find the minimum barrier width that is hydrophobic. Step 4: Find the minimum hydrophilic channel width that allows fluid to flow.

use a Xerox ColorQube 8570 wax printer (Rochester, NY, USA) and the paper we use is Whatman Grade 1 filter paper (Milwaukee, WI, USA). The second step is to use a heating source to melt and reflow the wax, which penetrates into the paper, forming a hydrophobic wax barrier. A Barnstead Thermolyne Cimarec top stirring hot plate (Dubuque, IA, USA) is used as the heating source. We should first calibrate the output of the printer before fabricating the 8-channel microfluidic devices with wax printing. Our calibration process includes four steps. An experimental flowchart of our calibration process is shown in Figure 1.

In Step 1 of calibration, we use a draft 8-channel pattern to determine the fabrication time and temperature recipe. The temperature range is from 70 to 200 degrees, with an increment of 10 degrees Celsius. The purpose of this step is to narrow down the temperature range that will melt solid ink and determine the perfect recipe for heating. Although our hot plate has its own temperature control, we also use a Flir TG54 thermometer (Wilsonville, OR, USA) to double check the temperature. After completing Step 1, we should pick three recipes with the best preliminary results for the draft patterns.

We then do quantitative measurements **in Step 2 of calibration**. We determine the width of vertical and horizontal wax strokes ranging from 100 um to 1000 um in 100 um increments before and after heating, by using the three temperature and time recipes we choose in step 1. Examples of wax stroke patterns designed with Adobe Illustrator are shown in Figures 2 (a) and (b). To take pictures of each wax stroke, we use a QEA PIAS – II Diginal Microscope (Billerica, MA, USA). We then use Otsu's method on the pictures of the wax strokes to determine thresholds for the images based on histograms of these images. If needed, pictures taken by the QEA PIAS – II Digital Microscope should be cropped before applying Otsu's method to ensure the two peaks on histograms are balanced. In Figure 2 (c), one can see an example of a wax stroke picture taken by the QEA PIAS – II Diginal Microscope. The histogram in Figure 2 (d) corresponds to the wax stroke picture. For this wax stroke histogram, 100 is selected as the threshold for binary thresholding, since this is approximately the middle point between the two peaks. With the binary image we get from binary thresholding, we then calculate the width of the wax strokes.

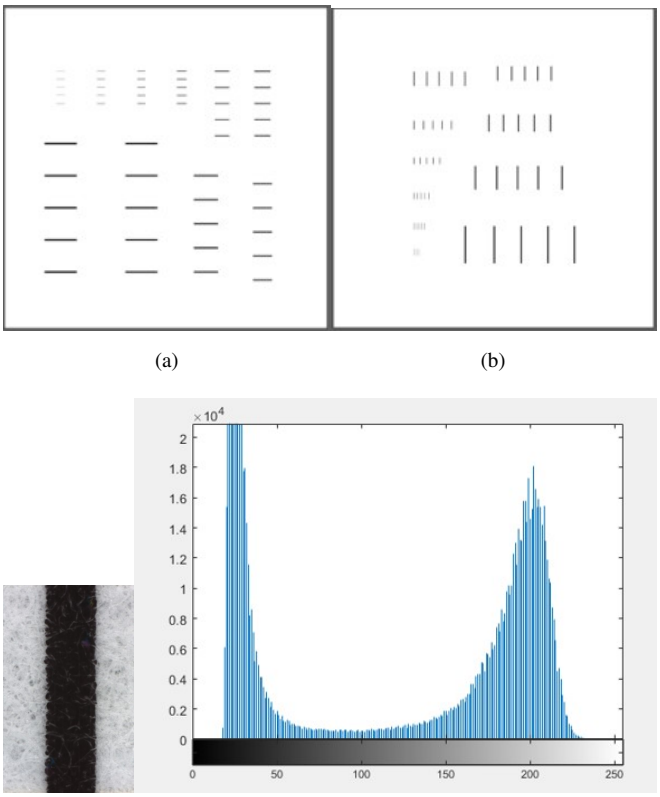

Figure 2: (a) and (b) Sample wax stroke patterns designed with Adobe Illustrator. (c) An example of wax stroke picture taken by QEA PIAS – II Diginal Microscope. (d) The corresponding histogram for (c).

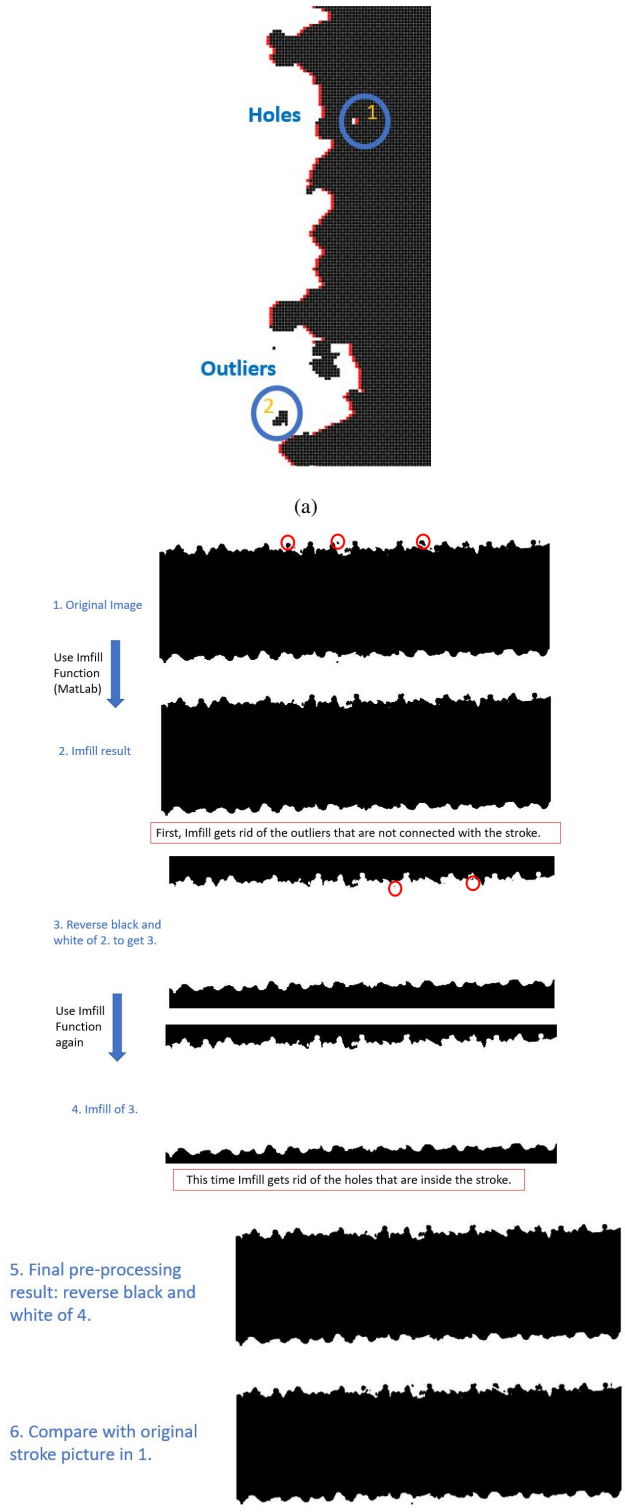

Figure 3: (a) and (b) Removal of two types of imperfections of a binary wax stroke picture, the first type are holes inside the stroke, the other type are outliers that are not connected with the main area of stroke.

Pre-processing Pipeline

Before we apply the code for width calculation, we need to do some pre-processing to eliminate the imperfections of the binary wax stroke images to make the width calculation easier and to make the results more accurate. There are generally two types of imperfections that may affect the width calculation of the binary stroke images. Figure 3 (a) illustrates the two types of imperfections: holes within the strokes, and outliers that are not connected to the main area of the strokes. In preprocessing, we aim to eliminate these two types of imperfections. Figure 3 (b) illustrates the entire preprocessing process applied to one binary stroke picture. During the preprocessing process, we used MatLab's Imfill function twice. A detailed description of this function can be found in [12]. First, we apply the Imfill function to the original binary picture (corresponding to Figure 3 (b) 1. 2.), which removes the outliers not connected to the main area of the stroke. This is because the Imfill function considers areas outside the picture as black background (corresponding to value 0). The stroke areas (black pixels) also correspond to value 0. The black outliers are within the white region, but they are unconnected to the stroke areas inside the picture or the background outside the picture, so they are forced to become white by the Imfill function based on connectivity. In the same vein, we can also use the imfill function to remove the white holes within the strokes, but we have to reverse the black and white pixels before using this method (corresponding to Figure 3 (b) 3. 4.). Finally, we reverse the black and white pixels again to complete the preprocessing (corresponding to 3 (b) 5.).

Width Calculation

Once we have completed pre-processing to remove white holes inside the stroke and black dots outside the stroke, we can calculate the width of the stroke. In order to calculate the width, we first apply least square fitting to fit a line to the left edge of a stroke, and then use the same method to fit a line to the right edge. After we get the least square fitting line for the two edges, we calculate the width of the stroke by computing the distance between the two least square fitting lines. With the width we computed, we can get two statistics: the average width, which is calculated based on 5 separate strokes; and the normalized standard deviation of the width of the 5 separate strokes, which is calculated based on the following equation:

$$\text{Normalized STDDEV} = \frac{\text{Standard Deviation}}{\text{Average Design Width}} \times 100\% \quad (1)$$

We select the optimal temperature and time to heat the wax printing samples based on the standard deviation of stroke width calculated in Step 2, and continue to use that temperature and time **in Step 3 of the calibration**. Step 3 deals with determining the minimum barrier width that is hydrophobic. Figure 1 Step 3 shows the pattern we use to determine the minimum hydrophobic barrier that works. We test both horizontal and vertical barriers with widths ranging from 100 um to 1000 um, incremented by 100 um. In the lab, we wait 30 minutes to confirm that the barriers are hydrophobic. To calculate the width of the barrier, we can use the same image processing pipeline we used in Step 2.

Then, in Step 4 of the calibration, we determine the minimum channel width that allows fluids to flow. The method for calculating the width of the channel is also similar to the image

processing pipeline in step 2. Figure 1 Step 4 shows the pattern we use to determine the minimum hydrophilic channel that works. The widths of the channels range from 100 um to 1000 um, in 100 um increments. Having completed all the steps of calibration, and we can utilize the information we have from Step 1-4 to update the 8-channel patterns.

Our device targets daily usage that is cost-effective for everyone, so we like to have multiple devices integrated on a single filter paper. The Whatman Grade 1 filter paper we are using comes in many sizes, the one we use is 200 mm $\times$ 200 mm. As our device has a 45 mm $\times$ 45 mm design dimension, we can integrate 4 $\times$ 4 or 16 devices on a single filter paper. Our final design for 8-channel devices has a channel width of 3 mm, which is determined based on standard deviation statistics of the channel width before and after heating. During the determination of the standard deviation, we compare two heating methods that are available to us: one is the hot plate (Barnstead Thermolyne Cimarec-Top Stirring Hot Plate) mentioned above, the other one is a heat gun (Maxwel Manufactoring, Victoria, Australia). We use patterns that have channels of different widths ranging from 1 mm to 4.5 mm with 0.5 mm increment, as shown in Figure 4. The width measurement method and standard deviation statistics calculation are similar to those in Step 2 of calibration.

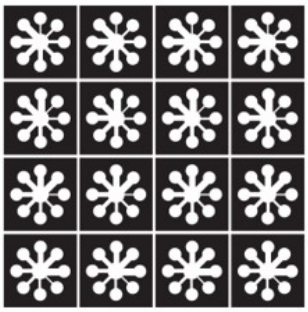

Figure 4: Pattern with channel widths ranging from 1 mm to 4.5 mm with 0.5 mm increments.

Lamination

It is also important to consider the lamination on the backside of the device, because without lamination, the solutions can leak to the backside of the paper. There are only hydrophobic barriers around the channels, but there is no lamination on the top or bottom of the device. Lamination can be accomplished in several different ways, the first is the use of a wax layer, which is mentioned in [10]. With this method, we should print the device with the wax printer, then heat it as usual, and then add another wax layer on the back surface of the device using the same wax printer. However, the second layer must not be heated, because if it is, then it will cover the entire device and ruin it. Another option is to use a lamination sheet. There are two types of lamination sheets: adhesive and hot seal. The adhesive lamination sheets work just like scotch tape, we can adhere them to the back or sides of the devices. Most hot seal lamination sheets are pouches, which are used to protect identification cards and important documents. Hot seal pouches of this type are designed to laminate both sides, but we cannot do that for our devices, as we should apply solutions from one side, so we only need the other side to be laminated. A procedure for laminating one side with a two-sided lamination pouch is described in [13]. By using this method, two pieces of paper (devices) are put inside the lamination pouch back-to-back. We should then laminate the pouch with a heat laminator and then cut the paper along the edges. The sides facing outward stick to laminating sheets, while the sides facing inward do not, so we end up with two single-side laminated paper devices.

Experiments and Results

Step 1 of Calibration

In the experiment, we noticed that heat is distributed unevenly on the hot plate. Only the middle area of the hot plate matches the temperature indicator, while the edges have a lower temperature. For this reason, we cut each single sheet of filter paper with a 4 $\times$ 4 array of devices into individual devices and place them on the hot plate. In the test, we started at 70 degrees Celsius and increased the temperature in 10 degree increments as designed. At 100 degrees Celsius, the wax melted, but there were some uneven spots on the backside of the paper, as shown in Figure 5(a). In the case of 100 degrees, the melting time was 2 minutes. When the device was heated at 150 degrees Celsius (Figure 5(b)), the wax melted in 11.86 seconds, which is a lot faster than when the device was heated at 100 degrees Celsius. At 170 degrees Celsius, the heating took only 6.38 seconds, as shown in Figure 5(c). As shown in Figure 5(d), at 190 degrees Celsius, the heating was ready within 5.36 seconds, which is even quicker. On the backside of the paper paper, there are tiny transparent water droplets. These droplets were used to roughly test the hydrophobic properties of the wax area. In the case that the wax printed areas are hydrophobic, the water droplets will remain there, while if the areas are not hydrophobic, water droplets will be absorbed by the filter paper. The heating time should not be too long, since the wax may flow into the channels, causing them to shrink dramatically. We therefore selected 150, 170, and 190 degrees Celsius at the end of Step 1, for a good wax flow result and a relatively rapid heating time.

Step 2 of Calibration

Using the three temperatures we chose from Step 1 as recipes to heat our wax printed samples, we conduct quantification experiments in Step 2 to determine stroke width. As mentioned in the Methods section, the average width is calculated using five separate testing samples, and the standard deviation is calculated using Equation (1). Using our image processing pipeline to calculate width, Figures 6 (a) and (b) show the average width and standard deviation for horizontal wax strips. Figures 6 (c) and (d) show the average width and standard deviation for vertical wax strips. As can be seen in the figure, the average widths of horizontal and vertical wax strips are very consistent. Table 1 shows the average normallized standard deviations for each temperature. In terms of standard deviation, 170 degrees Celsius stands out both for vertical and horizontal wax strips. Accordingly, we chose 170 degree Celsius from the three recipes, and this temperature were used for the rest of the calibration steps.

Step 3 of Calibration

During Step 3, we found out that the minimum design horizontal barrier that is hydrophobic is 300 um, while the actual average width of the barrier after it has been heated at 170 degree Celsius is 1039.1 um. The minimum design hydrophobic vertical

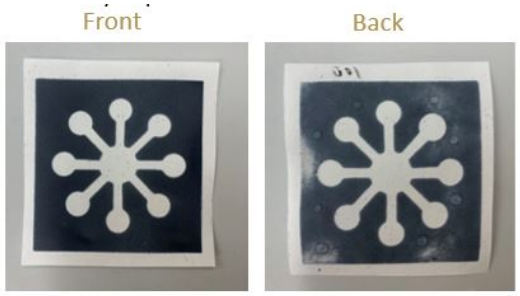

(a) 100 °C

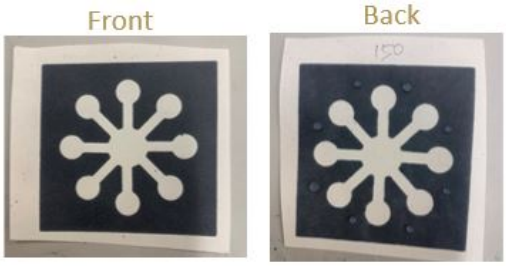

(b) 150 °C

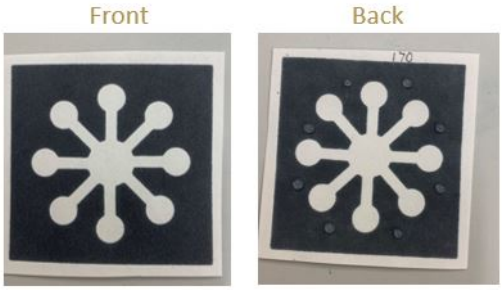

(c) 170 °C

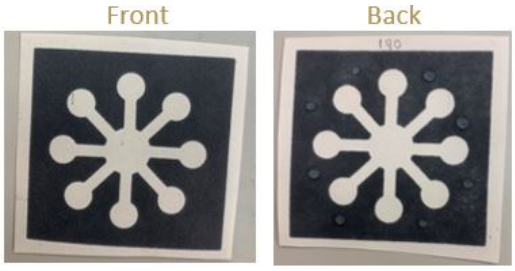

(d) 190 °C

Figure 5: The front and back of the paper device heated using different temperatures. The small spots on the backside of the devices that are located between each pair of pads are water droplets intended to test the hydrophobic properties of the backside wax coating.

barrier is 200 um, and the average width after heating is 1019.825 um. Figure 7 shows a few samples of working horizontal barriers.

Step 4 of Calibration

As a result of our work in Step 4, we know that the minimum channels to allow fluid flow have a design width of 900 um for

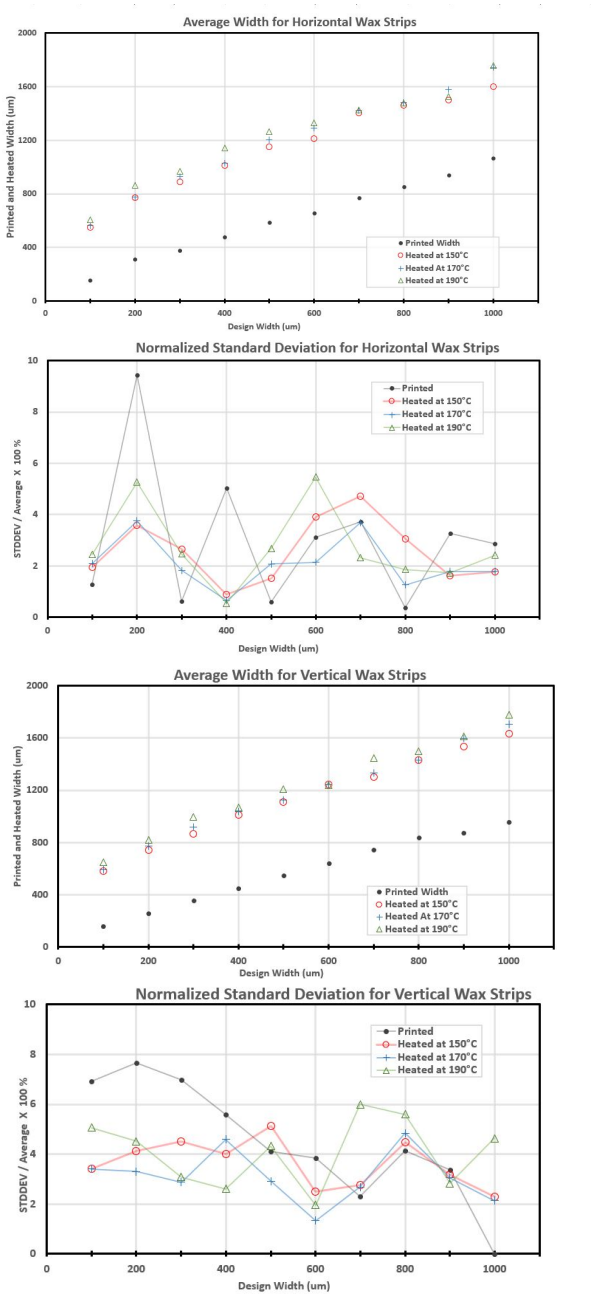

Figure 6: (a) and (b) Average width and normalized standard deviation for horizontal wax strips. (c) and (d) Average width and standard deviation for vertical wax strips.

	Average Normalized STDDEV (Horizontal)	Average Normalized STDDEV (Vertical)
150 ℃	25.600 %	36.337 %
170 ℃	21.029 %	31.089 %
190 ℃	27.176 %	40.570 %

Table 1: Average normalized standard deviation for channel widths shown in Figure 6.

horizontal channels. After heating, the channel width is approximately 207.292 um. The minimum vertical channels that allow

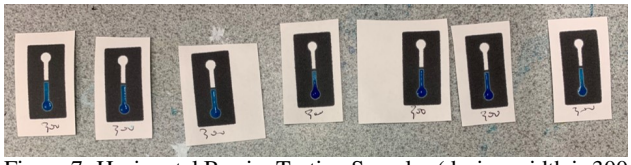

Figure 7: Horizontal Barrier Testing Samples (design width is 300 um).

fluid flow have a design width of 1000 um, and the after-heating width is around 259.375 um. Figure 8 shows a few samples of working vertical barriers. The after-heating width was measured with the same image processing pipeline as in Step 2. Due to too narrow channels after heating, selecting an appropriate threshold from the image histograms is difficult since there are not very obvious peaks. As a result, the after-heating width may not be as accurate as the width calculated in Step 2.

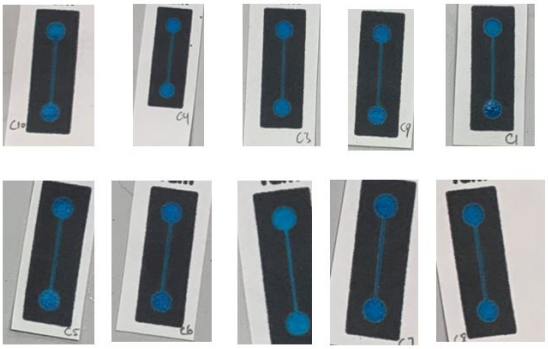

Figure 8: Vertical Channels Testing Samples (design width is 1000 um).

Heat Gun vs. Hot Plate

As mentioned in Step 1, we discovered that the hot plate has an uneven distribution of heat, so the filter paper had to be cut up into single devices to heat up. Alternatively, if we use a heat gun to heat the samples, we do not have to cut the paper. We can simply move the heat gun across the filter paper. For comparison of the two heating methods and to determine what channel width we should use, we fabricated the patterns described above in the Methods section and shown in Figure 4. We determined the channel width after heating in the same way as in Step 2. Figure 9 shows a comparison of the two heating methods, heat gun and hot plate, in terms of average width and normalized standard deviation. These statistics are based on each of the eight channels for each of the 16 devices on the printed page shown in Figure 4. Thus, they are an average over 128 separate measurements. The standard deviation statistics graph indicates that for widths smaller than 2000 um, the hot plate has a smaller batch to batch variation than the heat gun. Whereas the heat gun is better for widths greater than 2500 um since the variance between batches is reduced. Considering that we do not want to cut the filter paper, we chose 3000 um or 3 mm as our channel width, and the devices were heated by the heat gun.

Conclusions

This work proposed an eight-channel paper based microfluidic device fabricated using wax printing. Calibration of the wax

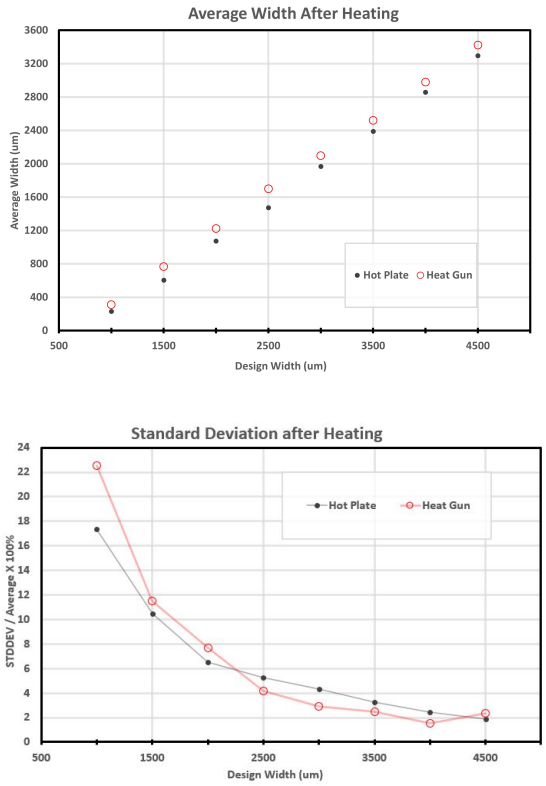

Figure 9: Average width and standard deviation statistics of testing samples after heating with heat gun and hot plate.

printing was performed in four steps, and our image processing pipeline was used to measure the width of wax strips and channels. Based on the standard deviation of the width we measured, we chose 170 degrees Celsius for heating. During the calibration, we observed that 300 um or wider horizontal barriers and 200 um or wider vertical barriers are hydrophobic and prevent liquid flow. A minimum width of 900 um is required for horizontal channels to allow fluid flow, while a minimum width of 1000 um is required for vertical channels to allow fluid flow. The final eight-channel device has a design channel width of 3 mm, and we can use a heat gun to heat the entire filter paper without cutting it into individual devices.

As we are waiting for our colleagues in Material Science to provide new samples with heavy metal particles, this work does not include colorimetric experiments. In future work, we may present our findings regarding the colorimetric response of heavy metal particles for our eight-channel devices.

For our previous publication [5], we used a photo booth in the fume hood to take pictures. We would eventually like to create an app on the smartphone that can be used to take pictures and detect the concentration of heavy metal particles using our paper device. Therefore, another research opportunity could involve enabling people to take pictures of paper devices without relying on a photo booth by removing the effect of different lighting conditions.

Acknowledgments

This manuscript is based upon work supported by the U.S. Department of Agriculture, Agricultural Research Service, under Agreement No. 59-8072-6-001. Any opinions, findings, conclusion, or recommendations expressed in this publication are those of the author(s) and do not necessarily reflect the view of the U.S. Department of Agriculture.

References

[1] D. Qin, Y. Xia, and G. M. Whitesides, "Soft lithography for micro-and nanoscale patterning," *Nature Protocols*, vol. 5, no. 3, pp. 491–502, 2010.

[2] G. M. Whitesides, E. Ostuni, S. Takayama, X. Jiang, and D. E. Ingber, "Soft lithography in biology and biochemistry," *Annual Review of Biomedical Engineering*, vol. 3, no. 1, pp. 335–373, 2001.

[3] M. Islam, R. Natu, and R. Martinez-Duarte, "A study on the limits and advantages of using a desktop cutter plotter to fabricate microfluidic networks," *Microfluidics and Nanofluidics*, vol. 19, no. 4, pp. 973–985, 2015.

[4] D. A. Bruzewicz, M. Reches, and G. M. Whitesides, "Low-cost printing of poly (dimethylsiloxane) barriers to define microchannels in paper," *Analytical Chemistry*, vol. 80, no. 9, pp. 3387–3392, 2008.

[5] M. Zhao, S. Diaz-Amaya, A. J. Deering, L. Stanciu, G. T.-C. Chiu, and J. P. Allebach, "Image analytics for food safety," *Proc. IMAWM*, 2020.

[6] E. Carrilho, A. W. Martinez, and G. M. Whitesides, "Understanding wax printing: a simple micropatterning process for paper-based microfluidics," *Analytical Chemistry*, vol. 81, no. 16, pp. 7091–7095, 2009.

[7] M. Younas, A. Maryam, M. Khan, A. A. Nawaz, S. H. I. Jaffery, M. N. Anwar, and L. Ali, "Parametric analysis of wax printing technique for fabricating microfluidic paper-based analytic devices (μpad) for milk adulteration analysis," *Microfluidics and Nanofluidics*, vol. 23, no. 3, pp. 1–10, 2019.

[8] G. G. Morbioli, N. C. Speller, M. E. Cato, T. P. Cantrell, and A. M. Stockton, "Rapid and low-cost development of microfluidic devices using wax printing and microwave treatment," *Sensors and Actuators B: Chemical*, vol. 284, pp. 650–656, 2019.

[9] A. Nilghaz, X. Liu, L. Ma, Q. Huang, and X. Lu, "Development of fabric-based microfluidic devices by wax printing," *Cellulose*, vol. 26, no. 5, pp. 3589–3599, 2019.

[10] E. B. Strong, C. Knutsen, J. T. Wells, A. R. Jangid, M. L. Mitchell, N. W. Martinez, and A. W. Martinez, "Wax-printed fluidic time delays for automating multi-step assays in paper-based microfluidic devices (micropads)," *Inventions*, vol. 4, no. 1, p. 20, 2019.

[11] N. Otsu, "A threshold selection method from gray-level histograms," *IEEE transactions on systems, man, and cybernetics*, vol. 9, no. 1, pp. 62–66, 1979.

[12] P. Soille, *Morphological image analysis: principles and applications*. Springer Science & Business Media, 2013.

[13] M. Morsa, "Resource center - how to 1-side laminate with a 2-side laminating pouch: Binding101.com: Binding101," Nov 2018.

Author Biography

Qiyue Liang is pursuing a Ph.D degree in electrical engineering at Purdue University under the supervision of Professor Jan P. Allebach. She received her B.S of science in electrical engineering degree from Purdue University(2018). Her current research interests include image processing and machine learning.

JOIN US AT THE NEXT EI!

IS&T International Symposium on

Electronic Imaging

SCIENCE AND TECHNOLOGY

Imaging across applications . . . Where industry and academia meet!

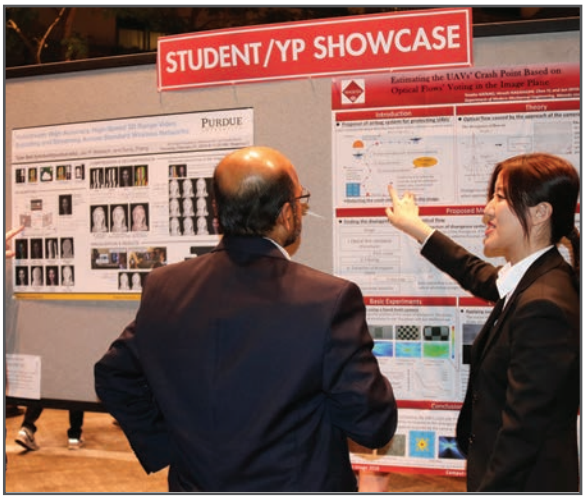

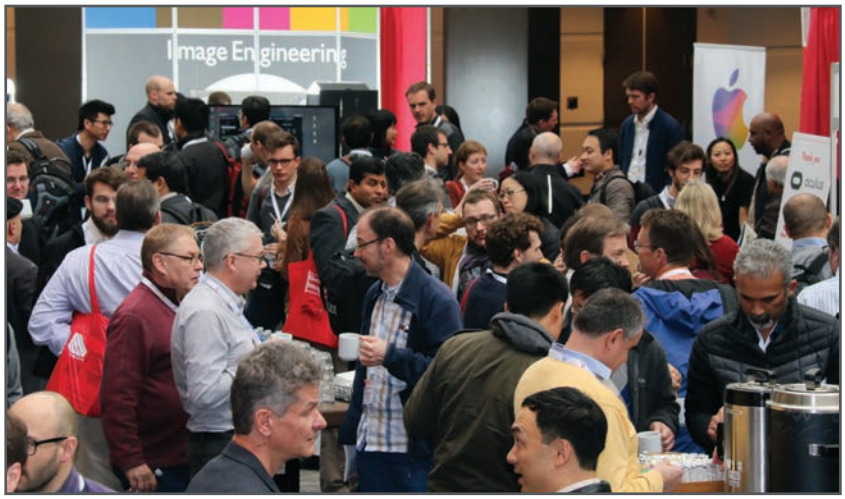

• SHORT COURSES • EXHIBITS • DEMONSTRATION SESSION • PLENARY TALKS •
• INTERACTIVE PAPER SESSION • SPECIAL EVENTS • TECHNICAL SESSIONS •

www.electronicimaging.org

IS&T
imaging.org